

Optimizing dynamical blockade via a particle-swarm-optimization algorithm

Guang-Yu Zhang,¹ Zhi-Hao Liu,¹ and Xun-Wei Xu^{1,2,*}

¹Key Laboratory of Low-Dimensional Quantum Structures and Quantum Control of Ministry of Education,
Key Laboratory for Matter Microstructure and Function of Hunan Province,
Department of Physics and Synergetic Innovation Center for Quantum Effects and Applications,
Hunan Normal University, Changsha 410081, China

²Institute of Interdisciplinary Studies, Hunan Normal University, Changsha 410081, China



(Received 29 April 2024; revised 25 June 2024; accepted 7 August 2024; published 16 August 2024)

Photon blockade in weak nonlinear regime is an exciting and promising subject that has been extensively studied in the steady state. However, how to achieve dynamic blockade in a *single* bosonic mode with *weak* nonlinearity using *only* pulsed driving field remains unexplored. Here, we propose to optimize the parameters of the pulsed driving field to achieve dynamic blockade in a single bosonic mode with weak nonlinearity via the particle swarm optimization (PSO) algorithm. We demonstrate that both Gaussian and rectangular pulses can be used to generate dynamic blockade in a single bosonic mode with weak nonlinearity. Based on the Fourier series expansions of the pulsed driving field, we identify that there are many paths for two-photon excitation in the bosonic mode, even only driven by pulsed field, and the dynamic blockade in a weak nonlinear regime is induced by the destructive interference between them. Our paper not only highlights the effectiveness of PSO algorithm in optimizing dynamical blockade but also opens a probable way to optimize the parameters for other quantum effects, such as quantum entanglement and quantum squeezing.

DOI: [10.1103/PhysRevA.110.023718](https://doi.org/10.1103/PhysRevA.110.023718)

I. INTRODUCTION

Photon blockade is a pure quantum effect that suppresses multiphoton generation in a bosonic mode [1]. It is a mechanism for the generation of single photons through coherent optical driving [2,3] and plays a pivotal role in the development of quantum computing [4,5], quantum networks [6,7], quantum cryptography [8,9], and quantum sensing [10,11]. Conventionally, photon blockade is proposed by introducing various strong nonlinear interactions into the optical modes [12–23] and has been observed in some experimental platforms, such as optical cavities coupled to single atoms [24–26], quantum dots embedded in photonic-crystal nanocavities [27,28], and superconducting qubits resonantly coupled to microwave resonators [29,30]. However, strong nonlinearity is still difficult to achieve in most experimental platforms, and photon blockade in weak nonlinear regime is an exciting and promising subject.

In the past decade, some novel mechanisms have been proposed to obtain photon blockade under weak nonlinear interactions. The one that attracts the most attention is the photon blockade originating from the suppression of two-photon excitation by destructive interference between different transition paths. It was first predicted in weakly nonlinear photonic molecules [31,32] and then observed for both optical [33] and microwave [34] photons. Photon blockade based on destructive interference has been extensively studied in various systems, such as coupled optomechanical systems [35–37], coupled cavities with second- or third-order

nonlinearities [38–51], cavity embedded with a quantum dot [52–56], coupled-resonator chain [57–59], etc. Photon blockade under weak nonlinear interactions has also been predicted in a bosonic mode with nonlinear driving [60,61] or nonlinear loss [62–65].

Different from the photon blockade predicted in the steady state by constant driving, dynamical blockade is a time-dependent phenomenon that strong photon blockade is achieved in certain periodic time windows. Dynamical blockade has been proposed in nonlinear systems driven by a coherent field with time-dependent amplitude [66–71] or using time-dependent coupling [72]. Due to the destructive interference between different paths for two-photon excitation, dynamical blockade has been predicted in the weakly nonlinear regime when a bosonic mode is coupled to two other modes by four-wave mixing [68], or coupled to a gain medium [69], or driven by a combination of continuous and pulsed fields [70], or driven by a bi-tone coherent field [71]. Nevertheless, how to achieve dynamic blockade in a single bosonic mode with weak nonlinearity driven by *only* a pulsed field is still an open question.

In this paper, we propose to optimize the parameters of the pulsed driving field to achieve a dynamic blockade in a single bosonic mode with weak nonlinearity via the particle swarm optimization (PSO) algorithm [73]. The PSO algorithm, inspired by collective behaviors observed in natural phenomena such as flocks of birds and schools of fish, operates as a group stochastic optimization algorithm, which has extensive applications in physics, such as crystal structure prediction [74], design of diffraction grating filters [75], maximization of topological invariants [76], characterization of dephasing quantum systems [77], and cosmological parameter

*Contact author: xwxu@hunnu.edu.cn

estimation [78]. Here, we apply the PSO algorithm to demonstrate dynamic blockade in a single bosonic mode with weak Kerr nonlinearity using *only* pulsed excitations. We optimize the parameters of the Gaussian and rectangular pulses by the PSO algorithm to generate strong dynamic blockade in a single bosonic mode with weak nonlinearity. The method of parameters optimization based on PSO algorithm is not only for achieving photon blockade but may also be applied to optimize the parameters for quantum entanglement [79] and quantum squeezing [80].

The paper is organized as follows. In Sec. II, we present the model of a single bosonic mode with Kerr nonlinearity driven by a pulsed coherent field, and briefly introduce the PSO algorithm. We demonstrate the dynamic blockade in a bosonic mode driven by a series of Gaussian pulses optimized by the PSO algorithm in Sec. III. In Sec. IV, we show that dynamic blockade also can be observed in the bosonic mode when it is driven by a series of optimized rectangular pulses. Finally, we make the conclusions in Sec. V.

II. MODEL AND ALGORITHM

A. Physical model

We consider a single bosonic mode with Kerr nonlinearity driven by a pulsed coherent field, and in the frame rotating with the driving frequency ω_d , the system can be described by the Hamiltonian ($\hbar = 1$)

$$H = \Delta a^\dagger a + U a^\dagger a^\dagger a a + \varepsilon(t)(a^\dagger + a), \quad (1)$$

where $a^\dagger(a)$ is the creation (annihilation) operator of the bosonic mode with the resonant frequency ω_a , U is the strength of nonlinearity, $\varepsilon(t)$ is the envelope of the pulsed driving field at time t , and $\Delta \equiv \omega_a - \omega_d$ is the detuning between the bosonic mode and driving field.

The dynamic of the system is governed by the quantum master equation [81]

$$\dot{\rho} = -i[H, \rho] + \frac{\gamma}{2}(2a\rho a^\dagger - a^\dagger a\rho - \rho a^\dagger a), \quad (2)$$

where ρ is the density matrix of the system and γ is the decay rate of the bosonic mode. The statistics of the bosonic mode can be evaluated by the instantaneous equal-time second-order correlation function

$$g^{(2)}(t) = \frac{\langle a^\dagger(t)a^\dagger(t)a(t)a(t) \rangle}{\langle a^\dagger(t)a(t) \rangle \langle a^\dagger(t)a(t) \rangle}, \quad (3)$$

which indicates dynamic blockade by $g^{(2)}(t) < 1$.

As the Hamiltonian is time dependent, except for a few cases (such as using a simple bi-tone drive [71]), it is hard to analytically obtain the optimal conditions for the dynamic blockade. Here, we try to overcome this challenge via an optimization algorithm widely used in artificial intelligence (see next subsection) and numerically demonstrate dynamic blockade in a single bosonic mode in the weak nonlinear regime, i.e., $U < \gamma$, driven *only* by pulsed coherent field. Without loss of generality, we set $U/\gamma = 0.05$ in the following numerical simulations.

B. Optimization algorithm

In this subsection, we briefly survey the optimization algorithm, i.e., the PSO algorithm, that we will use to optimize the parameters for achieving dynamic blockade in a single bosonic mode in the weak nonlinear regime. To be more specific, we will search for the optimal parameters of the pulsed driving field by the PSO algorithm to achieve the minimal second-order correlation function $g^{(2)}(t)$.

In the PSO algorithm, there are N_p computational agents, referred to as particles, without any relation to the physical particles. Each particle is assigned a position and a velocity vector. The position of the i th particle at the k th iteration ($k = 0, 1, 2, \dots, N_k$) is

$$X_i^k = [X_{i1}^k, X_{i2}^k, \dots, X_{id}^k]^T \quad (4)$$

and the velocity is

$$V_i^k = [V_{i1}^k, V_{i2}^k, \dots, V_{id}^k]^T, \quad (5)$$

where d denotes the dimensionality corresponding to the number of unknown parameters in the problem to be solved, and N_k is the maximum number of iterations. Here, we set particle number $N_p = 20$ and iteration number $N_k = 50$, and search for the optimized pulsed driving field to minimize $g^{(2)}(t)$. The parameters of the driving field, i.e., the detuning Δ and the parameters for the envelope of the driving field $\varepsilon(t)$, serve as the components of the position vector.

The positions of the particles are initiated by random numbers in a given range (described later), the initial values of the components in the velocities are initialized by random numbers within the range $[-0.1, 0.1]$, and the positions and velocities are updated at each iteration until an optimization position is obtained. At the $(k+1)$ th iteration, the position and velocity of the i th particle are updated in the following way:

$$X_i^{k+1} = X_i^k + V_i^{k+1}, \quad (6)$$

$$V_i^{k+1} = wV_i^k + f_1 r_1 (P_i^k - X_i^k) + f_2 r_2 (G^k - X_i^k). \quad (7)$$

Here, w represents the inertial weight, exerting a significant influence on the algorithm's search capability. A larger w promotes global exploration while a smaller w is conducive to local exploration. The parameters f_1 and f_2 correspond to the individual cognitive learning factor and social learning factor, respectively. Without loss of generality, we set $w = 0.5$ and $f_1 = f_2 = 1.5$ for numerical simulation. The random numbers r_1 and r_2 , sampled from the interval $[0,1]$, introduce an element of randomness to enhance the search process.

The quality of the position is characterized by a fitness value evaluated by an optimization function (fitness function) based on the predetermined criteria. In this paper, the fitness function is defined as the minimum of the instantaneous equal-time second-order correlation function, denoted by $g_{\min}^{(2)}(t)$, within a specified time range. The instantaneous equal-time second-order correlation function is calculated by numerically solving the master equation (2) with the open-source software QUTIP [82,83] for the system driven by a pulsed field characterized by d -dimensional parameters, i.e., the position X_i^k .

There are two kinds of historically best positions that should be memorized at each iteration. One is P_i^k , the

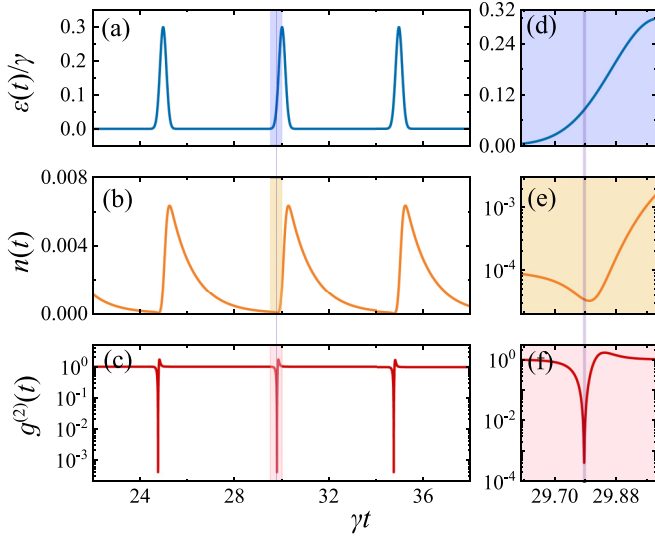


FIG. 1. (a) The envelope of the driving Gaussian pulses $\varepsilon(t)$, (b) the mean photon number $n(t)$, and (c) the equal-time second-order correlation function $g^{(2)}(t)$ versus time γt . (d)–(f) The local enlarged views of (a)–(c), respectively. The parameters are $U/\gamma = 0.05$, $\gamma T = 5$, $\Delta/\gamma = 0.5$, $\varepsilon_p/\gamma = 0.1$, and $A = 5.27$.

historically best position of the i th particle within k iterations for the fitness function $[g_{\min}^{(2)}(t)]$ achieving the minimal value, and the other one is G^k , the historically best position for the entire swarm within k iterations. When the particle's fitness value becomes approximately constant with the increasing iteration number, the optimization position is found and the corresponding best position G^k is the set of the optimized parameters of the driving field.

III. GAUSSIAN PULSES

As a specific example, we consider the case that the bosonic mode is driven by a series of Gaussian pulses in this section, and the envelope of the driving field is written as

$$\varepsilon(t) = \frac{\varepsilon_p A}{\sqrt{\pi}} \sum_m \exp[-A^2 \gamma^2 (t - mT)^2], \quad (8)$$

where ε_p denotes the driving strength, A governs the duration of the pulses, T represents the period of the pulses, and m is an integer. To optimize the parameters of the driving field for dynamic blockade, the position for the i th particle at the k th iteration is given by

$$X_i^k = [\Delta_i^k, \varepsilon_{p,i}^k, T_i^k, A_i^k]^T, \quad (9)$$

where Δ_i^k , $\varepsilon_{p,i}^k$, T_i^k , and A_i^k are the detuning, the driving strength, the period, and the duration of the pulses, respectively. The ranges of these parameters for optimization are set as follows: Δ/γ in the range $(-5, 5)$, ε_p/γ in the range $(0.1, 0.5)$, γT in the range $(3, 8)$, and A in the range $(0.001, 10)$.

After 50 iterations, we obtain the following optimal parameters for dynamic blockade: $\Delta/\gamma = 0.5$, $\varepsilon_p/\gamma = 0.1$, $\gamma T = 5$, and $A = 5.27$. The envelope of the pulses $\varepsilon(t)$ for the optimized parameters is shown in Fig. 1(a), and the corresponding mean photon number $n(t)$ and second-order correlation function $g^{(2)}(t)$ are shown in Figs. 1(b) and 1(c), respectively. The

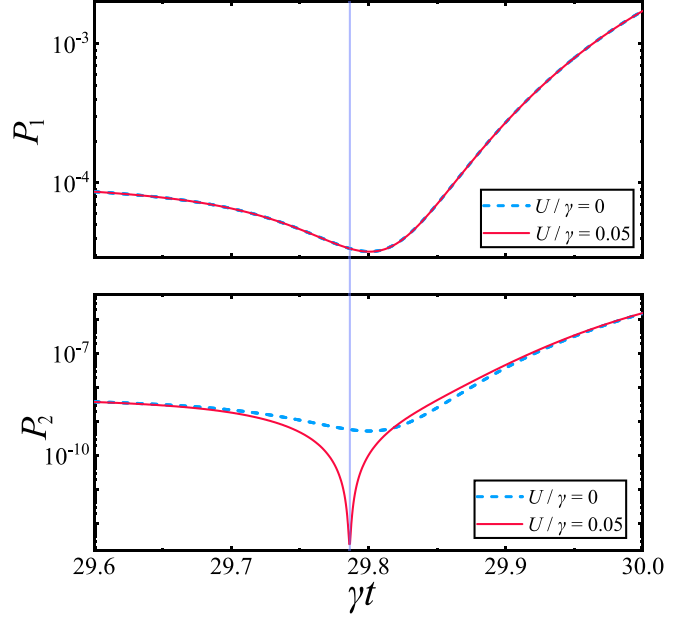


FIG. 2. The populations of Fock states with one photon and two photons (P_1 and P_2) versus time γt for $U = 0$ (blue dashed curves) and $U/\gamma = 0.05$ (red solid curves). The parameters are the same as in Fig. 1.

bosonic mode is periodically excited by the driving pulses, and there is a time delay between the driving pulses and the excitations [Figs. 1(d)–1(f)]. Such time delay induces a counterintuitive phenomenon that the decay of mean photon number is accelerated and the minimal mean photon number $n_{\min}(t) \approx 3 \times 10^{-4}$ [Fig. 1(e)] appears during the increasing of the driving strength (i.e., the rising edge of the driving pulse) [Fig. 1(d)]. Meanwhile, the second-order correlation function also decays rapidly in this regime and the strong antibunching is obtained with the minimum value $g_{\min}^{(2)}(t) \approx 4 \times 10^{-4}$ [Fig. 1(f)].

These phenomena can be understood based on the dynamics of the populations P_n of the Fock states $|n\rangle$ (n is a non-negative integer). The populations of Fock states with single photon (P_1) and two photons (P_2) are shown in Fig. 2 for $U = 0$ and $U = 0.05\gamma$. The decay of the populations (P_1 and P_2) is accelerated before they reach their minimal values. The single-photon excitation ($|0\rangle \rightarrow |1\rangle$) and two-photon excitation ($|1\rangle \rightarrow |2\rangle$) are suppressed by the destructive interference between different paths [see Fig. 3(c)], but the reverse transitions ($|1\rangle \rightarrow |0\rangle$ and $|2\rangle \rightarrow |1\rangle$) are enhanced by the driving field, which is the origin of the phenomenon that the decay of the mean photon number is accelerated at the rising edge of the driving pulse. If there is no nonlinear interaction ($U = 0$) in the bosonic mode, the dynamics of P_1 and P_2 are simultaneous, and there is no blockade effect, i.e., $2P_2/P_1^2 = 1$. In contrast, under the weak nonlinear interaction ($U = 0.05\gamma$), the dynamics of P_1 and P_2 become nonsimultaneous. After optimization, the two-photon excitation ($|1\rangle \rightarrow |2\rangle$) is suppressed much more seriously than the single-photon excitation ($|0\rangle \rightarrow |1\rangle$), which induces the results that the minimum value of P_2 is about four orders smaller than that for $U = 0$ and strong photon blockade is achieved at the rising edge of the driving pulse.

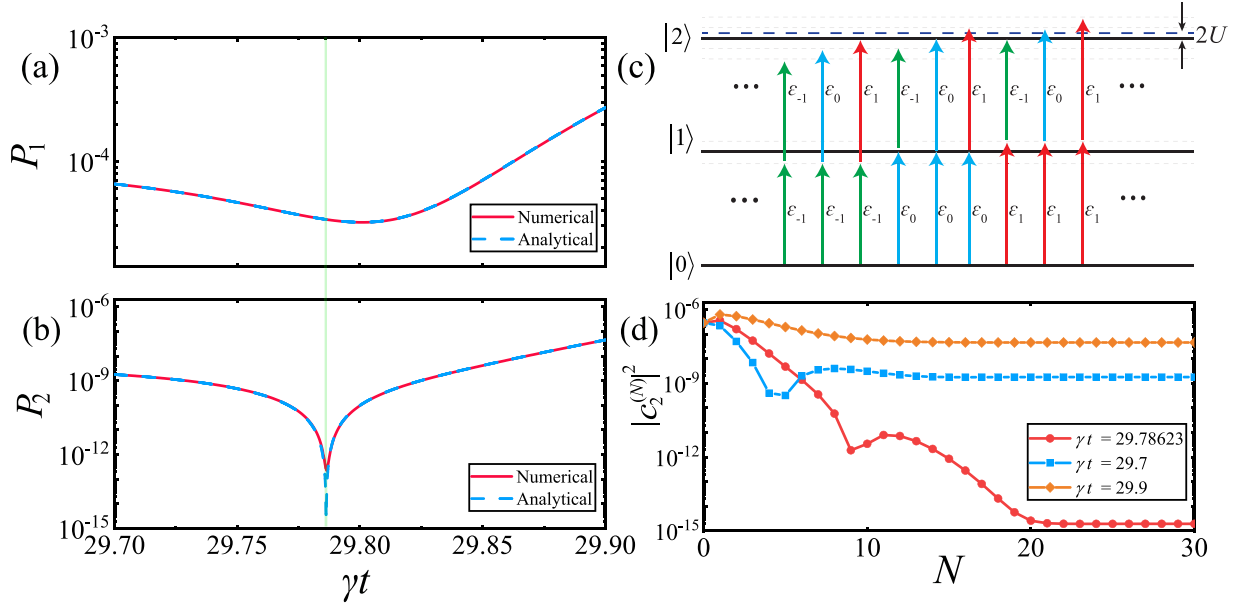


FIG. 3. The populations of Fock states $|1\rangle$ and $|2\rangle$ [(a) P_1 and (b) P_2] versus time γt by the numerical [Eq. (2)] (red solid curves) and analytical [Eqs. (15) and (16)] (blue dashed curves) methods. (c) Energy levels of a single bosonic mode with Kerr nonlinearity and the possible transition pathways for the bosonic mode driven by pulsed field [Eqs. (15) and (16)]. (d) $|c_2^{(N)}|^2$ versus N at different times ($\gamma t = 29.7, 29.78623, 29.9$). The parameters are the same as in Fig. 1.

To show the interference between different paths for two-photon excitation, we derive the populations of Fock states based on the Schrödinger equation. Under the weak excitation condition $n(t) \ll 1$, the state of the bosonic mode can be truncated to the two-photon manifold as

$$|\psi\rangle \approx c_0|0\rangle + c_1|1\rangle + c_2|2\rangle. \quad (10)$$

Here, $|n\rangle$ is the Fock state with n photons, and c_n is the corresponding coefficient that satisfies the conditions $|c_0| \approx 1 \gg |c_1| \gg |c_2|$. Based on the Schrödinger equation, $i\partial|\psi\rangle/\partial t = H_{\text{eff}}|\psi\rangle$, with the effective Hamiltonian $H_{\text{eff}} \equiv H - i\gamma a^\dagger a/2$, the dynamic equations for the coefficients c_1 and c_2 are given by

$$\frac{dc_1}{dt} = \left(-i\Delta - \frac{\gamma}{2}\right)c_1 - i\varepsilon(t), \quad (11)$$

$$\frac{dc_2}{dt} = [-i2(\Delta + U) - \gamma]c_2 - i\sqrt{2}\varepsilon(t)c_1. \quad (12)$$

The envelop of the pulsed driving field can be written as a Fourier series as

$$\varepsilon(t) = \sum_{k=-\infty}^{+\infty} \varepsilon_k \exp(ik\omega_p t), \quad (13)$$

where the complex coefficients are given by

$$\varepsilon_k = \frac{1}{T} \int_0^T \varepsilon(t) \exp(-ik\omega_p t) dt. \quad (14)$$

$\omega_p \equiv 2\pi/T$ is the generation frequency of the Gaussian-shaped pulses, and k is an integer. Following the method used

in Ref. [71], the dynamic equations can be solved via Fourier transformation as

$$c_1 = \sum_{k=-\infty}^{+\infty} \chi_k^{(1)} e^{ik\omega_p t}, \quad (15)$$

$$c_2 = \sum_{k'=-\infty}^{+\infty} \sum_{k=-\infty}^{+\infty} \chi_{k'k}^{(2)} \chi_k^{(1)} e^{i(k+k')\omega_p t}, \quad (16)$$

where

$$\chi_k^{(1)} = \frac{-i\varepsilon_k}{i(\Delta + k\omega_p) + \frac{\gamma}{2}}, \quad (17)$$

$$\chi_{k'k}^{(2)} = \frac{-i\sqrt{2}\varepsilon_{k'}}{[i(k+k')\omega_p + 2i(\Delta + U) + \gamma]}. \quad (18)$$

Based on the analytical solutions, the populations of Fock states $|1\rangle$ and $|2\rangle$ are given by $P_1 = |c_1|^2$ and $P_2 = |c_2|^2$.

The populations of Fock states $|1\rangle$ and $|2\rangle$ (P_1 and P_2) obtained by numerical [Eq. (2)] (red solid curves) and analytical [Eqs. (15) and (16)] (blue dashed curves) methods are shown in Figs. 3(a) and 3(b). The results obtained by these two methods match quantitatively. From Eq. (16), we can see that the two-photon excitation can be achieved through multiple paths, i.e., absorbing two photons with the same frequency ($k = k'$) or with different frequencies ($k \neq k'$), as shown in Fig. 3(c). All the paths for two-photon excitation may interfere destructively and lead to the vanishing of the population of Fock state $|2\rangle$ with $c_2 \approx 0$. To show the multiple-path destructive interference, we define

$$c_2^{(N)} = \sum_{k'=-N}^N \sum_{k=-N}^N \chi_{k'k}^{(2)} \chi_k^{(1)} e^{i(k+k')\omega_p t}, \quad (19)$$

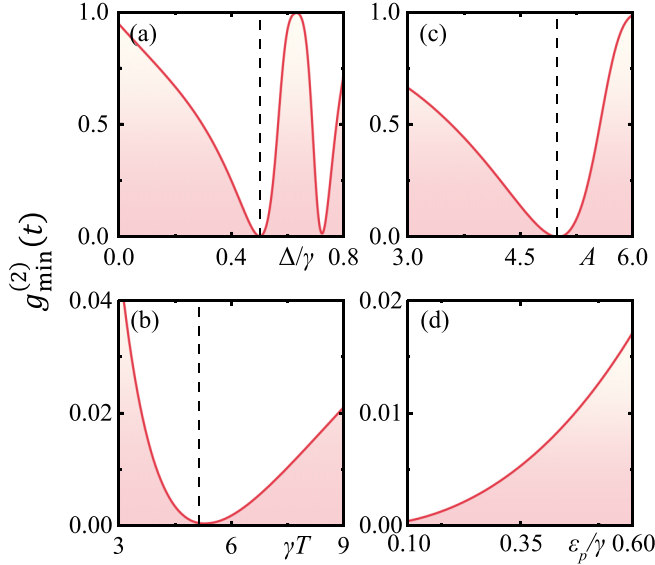


FIG. 4. The minimal values of the second-order correlation function $g_{\min}^{(2)}(t)$ versus parameters: (a) Δ/γ , (b) γT , (c) A , and (d) ε_p/γ . The other parameters are the same as in Fig. 1.

and we have $c_2^{(N)} = c_2$ for $N \rightarrow +\infty$. We show $|c_2^{(N)}|^2$ versus N , i.e., $(2N+1)^2$ paths, at different times in Fig. 3(d). It is clear that $|c_2^{(N)}|^2$ decreases gradually with the increase of N , and approaches to the stable value (P_2) for $N > 20$.

To demonstrate the optimization based on the PSO algorithm, we show the minimal values of the second-order correlation function $g_{\min}^{(2)}(t)$ versus the parameters of the driving pulses in Fig. 4. From these figures, we can see that the parameters ($\Delta/\gamma = 0.5$, $\gamma T = 5$, and $A = 5.27$) are indeed the optimal parameters for dynamic blockade, which indicates that the PSO algorithm can be used to obtain the optimal conditions for the dynamic blockade. In addition, there are some notes that should be mentioned: (i) As shown in Fig. 4(d), a smaller ε_p corresponds to a smaller $g_{\min}^{(2)}(t)$, as well as a smaller mean photon number $n(t)$. (ii) In the optimization, we set the range for γT as (3,8) because it is related to the mean photon number $n(t)$. A longer interval between two pulses results in a smaller mean photon number for strong dynamic blockade, so we impose an upper limit on γT to prevent a too small mean photon number. (iii) There are many optimal parameter regimes for strong dynamic blockade, so we can choose different parameters according to the experimental conditions and application situations.

IV. RECTANGULAR PULSES

The dynamic blockade optimization based on the PSO algorithm can be applied to the cases that the bosonic mode is driven by a pulsed field with different envelope. Rectangular pulses are also commonly used in optical driving, and there are even more controllable parameters for the envelope of the rectangular pulses, in comparing with the Gaussian pulses. In this section, we discuss the dynamic blockade optimization achieved by driving the bosonic mode with a series of rectangular pulses. The envelope of the rectangular pulses is written

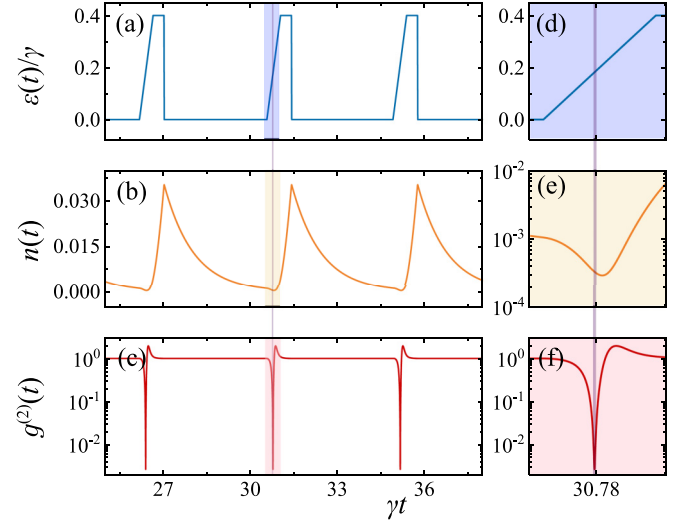


FIG. 5. (a) The envelope of the driving rectangular pulses $\varepsilon(t)$, (b) the mean photon number $n(t)$, and (c) the equal-time second-order correlation function $g^{(2)}(t)$ versus time γt . (d)–(f) The local enlarged views of (a)–(c), respectively. The parameters are $U/\gamma = 0.05$, $\Delta/\gamma = 0.617$, $\varepsilon_m/\gamma = 0.4$, $\gamma t_r = 0.468$, $\gamma t_w = 0.372$, $\gamma t_f = 0.01$, and $\gamma T = 4.365$.

as a function of time t as

$$\varepsilon(t) = \begin{cases} \varepsilon_m \frac{t'}{t_r}, & 0 \leq t' < t_r \\ \varepsilon_m, & t_r \leq t' < t_2 \\ \varepsilon_m \frac{(t_3 - t')}{t_f}, & t_2 \leq t' < t_3 \\ 0, & t_3 < t' < T, \end{cases} \quad (20)$$

where ε_m represents the maximal amplitude of the rectangular pulses, t_r designates the pulse rise time, t_f corresponds to the pulse fall time, t_w signifies the pulse width, T stands for the pulse period, $t_2 \equiv t_r + t_w$, $t_3 \equiv t_r + t_w + t_f$, $t' \equiv t\%T$, and $\%$ denotes the modulo operation.

To optimize the parameters of the rectangular pulses for dynamic blockade, the position for the i th particle at the k th iteration is given by

$$X_i^k = [\Delta_i^k, T_i^k, \varepsilon_{m,i}^k, t_{r,i}^k, t_{w,i}^k, t_{f,i}^k]^T, \quad (21)$$

where Δ_i^k , T_i^k , $\varepsilon_{m,i}^k$, $t_{r,i}^k$, $t_{w,i}^k$, and $t_{f,i}^k$ are the detuning, the period, the driving strength, the rise time, the width, and the fall time of the pulses, respectively. We set the range of the parameters as Δ/γ in the range $(-5, 5)$, γT in the range $(3, 8)$, ε_m/γ in the range $(0.4, 0.5)$, γt_r in the range $(0.01, 0.5)$, γt_w in the range $(0.01, 0.5)$, and γt_f in the range $(0.01, 0.5)$. The fitness value becomes stable after 50 iterations, yielding the optimal parameters for dynamic blockade: $\Delta/\gamma = 0.617$, $\varepsilon_m/\gamma = 0.4$, $\gamma t_r = 0.468$, $\gamma t_w = 0.372$, $\gamma t_f = 0.01$, and $\gamma T = 4.365$. The envelope of the rectangular pulses $\varepsilon(t)$, the mean photon number $n(t)$, and the second-order correlation function $g^{(2)}(t)$ plotted as functions of time t with the optimal parameters are shown in Fig. 5. The minimal mean photon number ($\approx 4 \times 10^{-4}$) [Fig. 5(e)] is achieved at the rising edges of the rectangular pulses [Fig. 5(d)], and the dynamic blockade with a minimal value of $g_{\min}^{(2)}(t) \approx 4 \times 10^{-3}$ [Fig. 5(f)] is obtained just before the mean photon number reaching its minimum value. As mentioned in the case of Gaussian pulses, the

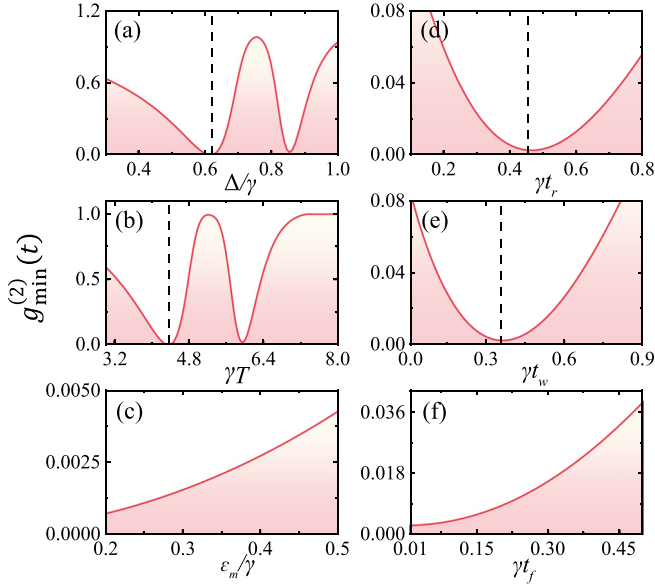


FIG. 6. The minimal values of the second-order correlation function $g_{\min}^{(2)}(t)$ versus parameters: (a) Δ/γ , (b) γT , (c) ε_m/γ , (d) γt_r , (e) γt_w , and (f) γt_f . The parameters are the same as in Fig. 5.

dynamic blockade in the weak nonlinear bosonic mode with pulsed driving is induced by the destructive interference between different paths for two-photon excitation [see Eq. (16)].

To demonstrate the results of optimization, we show the minimal values of the second-order correlation function $g_{\min}^{(2)}(t)$ versus one of the parameters, with the other optimal parameters fixed, in Fig. 6. It should be noted that there is no optimal values of both ε_m and t_f , i.e., a smaller $g_{\min}^{(2)}(t)$ is obtained with a smaller ε_m and t_f . Moreover, there are many minimal values in Figs. 6(a) and 6(b), which means that, besides the parameters in Fig. 5, there are some other parameter regimes that can also be used to achieve dynamic blockade.

V. CONCLUSIONS

In conclusion, we have proposed a scheme to optimize the envelopes of the driving pulses to generate strong photon blockade by the PSO algorithm and demonstrated dynamic blockade in a single bosonic mode with weak Kerr nonlinearity using only pulsed driving fields. Based on the analytical expression of the populations of Fock states, we found that there are many paths for two-photon excitation and the destructive interference between them induces the dynamic blockade in the weak nonlinear regime. Dynamic blockade optimization can be realized by different types of pulses based on the PSO algorithm, and we have shown the cases of driving the single bosonic mode with Gaussian or rectangular pulses. Our work opens a way to generate dynamic blockade by the optimization algorithm.

The PSO algorithm may be applied to optimize the parameters for observing other quantum effects. For example, we note that quantum entanglement and quantum squeezing have been extensively studied in the standard optomechanical systems driven by constant fields [84], but how to optimize the dynamic quantum entanglement and squeezing in a standard optomechanical system driven by pulsed fields is still an open question. The PSO algorithm for dynamic blockade proposed here may be generalized to optimize the parameters of the pulsed fields for exploring dynamic quantum entanglement and squeezing in a standard optomechanical system by replacing the fitness function with the log negativity (for entanglement) or quadrature fluctuations (for squeezing).

ACKNOWLEDGMENTS

This work is supported by the National Natural Science Foundation of China (NSFC) (Grants No. 12064010 and No. 12247105), the Science and Technology Innovation Program of Hunan Province (Grant No. 2022RC1203), and Hunan provincial major sci-tech program (Grant No. 2023ZJ1010).

- [1] A. Imamoglu, H. Schmidt, G. Woods, and M. Deutsch, Strongly interacting photons in a nonlinear cavity, *Phys. Rev. Lett.* **79**, 1467 (1997).
- [2] S. Buckley, K. Rivoire, and J. Vučković, Engineered quantum dot single-photon sources, *Rep. Prog. Phys.* **75**, 126503 (2012).
- [3] P. Lodahl, S. Mahmoodian, and S. Stobbe, Interfacing single photons and single quantum dots with photonic nanostructures, *Rev. Mod. Phys.* **87**, 347 (2015).
- [4] E. Knill, R. Laflamme, and G. J. Milburn, A scheme for efficient quantum computation with linear optics, *Nature (London)* **409**, 46 (2001).
- [5] P. Kok, W. J. Munro, K. Nemoto, T. C. Ralph, J. P. Dowling, and G. J. Milburn, Linear optical quantum computing with photonic qubits, *Rev. Mod. Phys.* **79**, 135 (2007).
- [6] H. J. Kimble, The quantum internet, *Nature (London)* **453**, 1023 (2008).
- [7] A. Reiserer and G. Rempe, Cavity-based quantum networks with single atoms and optical photons, *Rev. Mod. Phys.* **87**, 1379 (2015).
- [8] V. Scarani, H. Bechmann-Pasquinucci, N. J. Cerf, M. Dušek, N. Lütkenhaus, and M. Peev, The security of practical quantum key distribution, *Rev. Mod. Phys.* **81**, 1301 (2009).
- [9] F. Xu, X. Ma, Q. Zhang, H.-K. Lo, and J.-W. Pan, Secure quantum key distribution with realistic devices, *Rev. Mod. Phys.* **92**, 025002 (2020).
- [10] C. L. Degen, F. Reinhard, and P. Cappellaro, Quantum sensing, *Rev. Mod. Phys.* **89**, 035002 (2017).
- [11] S. Pirandola, B. R. Bardhan, T. Gehring, C. Weedbrook, and S. Lloyd, Advances in photonic quantum sensing, *Nat. Photon* **12**, 724 (2018).
- [12] A. Ridolfo, M. Leib, S. Savasta, and M. J. Hartmann, Photon blockade in the ultrastrong coupling regime, *Phys. Rev. Lett.* **109**, 193602 (2012).
- [13] Y.-X. Liu, X.-W. Xu, A. Miranowicz, and F. Nori, From blockade to transparency: Controllable photon transmission through a circuit-qed system, *Phys. Rev. A* **89**, 043818 (2014).
- [14] A. Miranowicz, J. Bajer, M. Paprzycka, Y.-X. Liu, A. M. Zagoskin, and F. Nori, State-dependent photon blockade via

- quantum-reservoir engineering, *Phys. Rev. A* **90**, 033831 (2014).
- [15] P. Rabl, Photon blockade effect in optomechanical systems, *Phys. Rev. Lett.* **107**, 063601 (2011).
- [16] A. Nunnenkamp, K. Børkje, and S. M. Girvin, Single-photon optomechanics, *Phys. Rev. Lett.* **107**, 063602 (2011).
- [17] J.-Q. Liao and F. Nori, Photon blockade in quadratically coupled optomechanical systems, *Phys. Rev. A* **88**, 023853 (2013).
- [18] H. Xie, G.-W. Lin, X. Chen, Z.-H. Chen, and X.-M. Lin, Single-photon nonlinearities in a strongly driven optomechanical system with quadratic coupling, *Phys. Rev. A* **93**, 063860 (2016).
- [19] A. Majumdar and D. Gerace, Single-photon blockade in doubly resonant nanocavities with second-order nonlinearity, *Phys. Rev. B* **87**, 235319 (2013).
- [20] R. Huang, A. Miranowicz, J.-Q. Liao, F. Nori, and H. Jing, Nonreciprocal photon blockade, *Phys. Rev. Lett.* **121**, 153601 (2018).
- [21] R. Huang, Ş. K. Özdemir, J.-Q. Liao, F. Minganti, L.-M. Kuang, F. Nori, and H. Jing, Exceptional photon blockade: Engineering photon blockade with chiral exceptional points, *Laser Photonics Rev.* **16**, 2100430 (2022).
- [22] S. Chakram, K. He, A. V. Dixit, A. E. Oriani, R. K. Naik, N. Leung, H. Kwon, W.-L. Ma, L. Jiang, and D. I. Schuster, Multimode photon blockade, *Nat. Phys.* **18**, 879 (2022).
- [23] Y. H. Zhou, X. Y. Zhang, Q. C. Wu, B. L. Ye, Z.-Q. Zhang, D. D. Zou, H. Z. Shen, and C.-P. Yang, Conventional photon blockade with a three-wave mixing, *Phys. Rev. A* **102**, 033713 (2020).
- [24] K. M. Birnbaum, A. Boca, R. Miller, A. D. Boozer, T. E. Northup, and H. J. Kimble, Photon blockade in an optical cavity with one trapped atom, *Nature (London)* **436**, 87 (2005).
- [25] B. Dayan, A. S. Parkins, T. Aoki, E. P. Ostby, K. J. Vahala, and H. J. Kimble, A photon turnstile dynamically regulated by one atom, *Science* **319**, 1062 (2008).
- [26] T. Aoki, A. S. Parkins, D. J. Alton, C. A. Regal, B. Dayan, E. Ostby, K. J. Vahala, and H. J. Kimble, Efficient routing of single photons by one atom and a microtoroidal cavity, *Phys. Rev. Lett.* **102**, 083601 (2009).
- [27] A. Faraon, I. Fushman, D. Englund, N. Stoltz, P. Petroff, and J. Vučković, Coherent generation of nonclassical light on a chip via photon-induced tunneling and blockade, *Nat. Phys.* **4**, 859 (2008).
- [28] A. Reinhard, T. Volz, M. Winger, A. Badolato, K. J. Hennessy, E. L. Hu, and A. Imamoglu, Strongly correlated photons on a chip, *Nat. Photon.* **6**, 93 (2012).
- [29] C. Lang, D. Bozyigit, C. Eichler, L. Steffen, J. M. Fink, A. A. Abdumalikov, M. Baur, S. Filipp, M. P. da Silva, A. Blais, and A. Wallraff, Observation of resonant photon blockade at microwave frequencies using correlation function measurements, *Phys. Rev. Lett.* **106**, 243601 (2011).
- [30] A. J. Hoffman, S. J. Srinivasan, S. Schmidt, L. Spietz, J. Aumentado, H. E. Türeci, and A. A. Houck, Dispersive photon blockade in a superconducting circuit, *Phys. Rev. Lett.* **107**, 053602 (2011).
- [31] T. C. H. Liew and V. Savona, Single photons from coupled quantum modes, *Phys. Rev. Lett.* **104**, 183601 (2010).
- [32] M. Bamba, A. Imamoglu, I. Carusotto, and C. Ciuti, Origin of strong photon antibunching in weakly nonlinear photonic molecules, *Phys. Rev. A* **83**, 021802(R) (2011).
- [33] H. J. Snijders, J. A. Frey, J. Norman, H. Flayac, V. Savona, A. C. Gossard, J. E. Bowers, M. P. van Exter, D. Bouwmeester, and W. Löffler, Observation of the unconventional photon blockade, *Phys. Rev. Lett.* **121**, 043601 (2018).
- [34] C. Vaneph, A. Morvan, G. Aiello, M. Féchant, M. Aprili, J. Gabelli, and J. Estève, Observation of the unconventional photon blockade in the microwave domain, *Phys. Rev. Lett.* **121**, 043602 (2018).
- [35] X.-W. Xu and Y.-J. Li, Antibunching photons in a cavity coupled to an optomechanical system, *J. Phys. B: At. Mol. Opt. Phys.* **46**, 035502 (2013).
- [36] V. Savona, Unconventional photon blockade in coupled optomechanical systems, [arXiv:1302.5937](https://arxiv.org/abs/1302.5937).
- [37] W.-Z. Zhang, J. Cheng, J.-Y. Liu, and L. Zhou, Controlling photon transport in the single-photon weak-coupling regime of cavity optomechanics, *Phys. Rev. A* **91**, 063836 (2015).
- [38] S. Ferretti, V. Savona, and D. Gerace, Optimal antibunching in passive photonic devices based on coupled nonlinear resonators, *New J. Phys.* **15**, 025012 (2013).
- [39] H. Flayac and V. Savona, Input-output theory of the unconventional photon blockade, *Phys. Rev. A* **88**, 033836 (2013).
- [40] D. Gerace and V. Savona, Unconventional photon blockade in doubly resonant microcavities with second-order nonlinearity, *Phys. Rev. A* **89**, 031803(R) (2014).
- [41] X.-W. Xu and Y. Li, Tunable photon statistics in weakly nonlinear photonic molecules, *Phys. Rev. A* **90**, 043822 (2014).
- [42] X.-W. Xu and Y. Li, Strong photon antibunching of symmetric and antisymmetric modes in weakly nonlinear photonic molecules, *Phys. Rev. A* **90**, 033809 (2014).
- [43] M.-A. Lemonde, N. Didier, and A. A. Clerk, Antibunching and unconventional photon blockade with Gaussian squeezed states, *Phys. Rev. A* **90**, 063824 (2014).
- [44] H. Z. Shen, Y. H. Zhou, and X. X. Yi, Tunable photon blockade in coupled semiconductor cavities, *Phys. Rev. A* **91**, 063808 (2015).
- [45] Y. H. Zhou, H. Z. Shen, and X. X. Yi, Unconventional photon blockade with second-order nonlinearity, *Phys. Rev. A* **92**, 023838 (2015).
- [46] H. Flayac and V. Savona, Unconventional photon blockade, *Phys. Rev. A* **96**, 053810 (2017).
- [47] B. Sarma and A. K. Sarma, Quantum-interference-assisted photon blockade in a cavity via parametric interactions, *Phys. Rev. A* **96**, 053827 (2017).
- [48] Y. H. Zhou, F. Minganti, W. Qin, Q.-C. Wu, J.-L. Zhao, Y.-L. Fang, F. Nori, and C.-P. Yang, n -photon blockade with an n -photon parametric drive, *Phys. Rev. A* **104**, 053718 (2021).
- [49] S. Shen, Y. Qu, J. Li, and Y. Wu, Tunable photon statistics in parametrically amplified photonic molecules, *Phys. Rev. A* **100**, 023814 (2019).
- [50] E. Z. Casalengua, J. C. López Carreño, F. P. Laussy, and E. d. Valle, Conventional and unconventional photon statistics, *Laser Photonics Rev.* **14**, 1900279 (2020).
- [51] D.-Y. Wang, C.-H. Bai, S. Liu, S. Zhang, and H.-F. Wang, Photon blockade in a double-cavity optomechanical system with nonreciprocal coupling, *New J. Phys.* **22**, 093006 (2020).
- [52] A. Majumdar, M. Bajcsy, A. Rundquist, and J. Vučković, Loss-enabled sub-Poissonian light generation in a bimodal nanocavity, *Phys. Rev. Lett.* **108**, 183601 (2012).

- [53] W. Zhang, Z. Yu, Y. Liu, and Y. Peng, Optimal photon antibunching in a quantum-dot-bimodal-cavity system, *Phys. Rev. A* **89**, 043832 (2014).
- [54] J. Tang, W. Geng, and X. Xu, Quantum interference induced photon blockade in a coupled single quantum dot-cavity system, *Sci. Rep.* **5**, 9252 (2015).
- [55] X. Liang, Z. Duan, Q. Guo, C. Liu, S. Guan, and Y. Ren, Antibunching effect of photons in a two-level emitter-cavity system, *Phys. Rev. A* **100**, 063834 (2019).
- [56] O. Kyriienko, D. N. Krizhanovskii, and I. A. Shelykh, Nonlinear quantum optics with trion polaritons in 2D monolayers: Conventional and unconventional photon blockade, *Phys. Rev. Lett.* **125**, 197402 (2020).
- [57] Y. Wang, W. Verstraelen, B. Zhang, T. C. H. Liew, and Y. D. Chong, Giant enhancement of unconventional photon blockade in a dimer chain, *Phys. Rev. Lett.* **127**, 240402 (2021).
- [58] J. Li, C.-M. Hu, and Y. Yang, Enhancement of photon blockade via topological edge states, *Phys. Rev. Appl.* **21**, 034058 (2024).
- [59] Z.-G. Lu, Y. Wu, and X.-Y. Lü, Chiral interaction induced near-perfect photon blockade, [arXiv:2402.09000](https://arxiv.org/abs/2402.09000).
- [60] A. Lingenfelter, D. Roberts, and A. A. Clerk, Unconditional Fock state generation using arbitrarily weak photonic nonlinearities, *Sci. Adv.* **7**, eabj1916 (2021).
- [61] Y.-X. Ma and P.-B. Li, Deterministic generation of phononic Fock states via weak nonlinearities, *Phys. Rev. A* **108**, 053709 (2023).
- [62] Y.-H. Zhou, X.-Y. Zhang, T. Liu, Q.-C. Wu, Z.-C. Shi, H.-Z. Shen, and C.-P. Yang, Environmentally induced photon blockade via two-photon absorption, *Phys. Rev. Appl.* **18**, 064009 (2022).
- [63] X. Su, J.-S. Tang, and K. Xia, Nonlinear dissipation-induced photon blockade, *Phys. Rev. A* **106**, 063707 (2022).
- [64] A. Ben-Asher, A. I. Fernández-Domínguez, and J. Feist, Non-Hermitian anharmonicity induces single-photon emission, *Phys. Rev. Lett.* **130**, 243601 (2023).
- [65] Y. Zuo, R. Huang, L.-M. Kuang, X.-W. Xu, and H. Jing, Loss-induced suppression, revival, and switch of photon blockade, *Phys. Rev. A* **106**, 043715 (2022).
- [66] G. Y. Kryuchkyan, A. R. Shahinyan, and I. A. Shelykh, Quantum statistics in a time-modulated exciton-photon system, *Phys. Rev. A* **93**, 043857 (2016).
- [67] G. H. Hovsepyan, A. R. Shahinyan, and G. Y. Kryuchkyan, Multiphoton blockades in pulsed regimes beyond stationary limits, *Phys. Rev. A* **90**, 013839 (2014).
- [68] O. Kyriienko and T. C. H. Liew, Triggered single-photon emitters based on stimulated parametric scattering in weakly nonlinear systems, *Phys. Rev. A* **90**, 063805 (2014).
- [69] S. Ghosh and T. C. H. Liew, Single photons from a gain medium below threshold, *Phys. Rev. B* **97**, 241301(R) (2018).
- [70] S. Ghosh and T. C. H. Liew, Dynamical blockade in a single-mode bosonic system, *Phys. Rev. Lett.* **123**, 013602 (2019).
- [71] M. Li, Y.-L. Zhang, S.-H. Wu, C.-H. Dong, X.-B. Zou, G.-C. Guo, and C.-L. Zou, Single-mode photon blockade enhanced by bi-tone drive, *Phys. Rev. Lett.* **129**, 043601 (2022).
- [72] D. Stefanatos and E. Paspalakis, Dynamical blockade in a bosonic Josephson junction using optimal coupling, *Phys. Rev. A* **102**, 013716 (2020).
- [73] J. Kennedy and R. Eberhart, Particle swarm optimization, *IEEE Int. Conf. Neural Networks* **4**, 1942 (1995).
- [74] Y. Wang, J. Lv, L. Zhu, and Y. Ma, Crystal structure prediction via particle-swarm optimization, *Phys. Rev. B* **82**, 094116 (2010).
- [75] M. Shokooh-Saremi and R. Magnusson, Particle swarm optimization and its application to the design of diffraction grating filters, *Opt. Lett.* **32**, 894 (2007).
- [76] S. Zhang and J. Gong, Floquet engineering with particle swarm optimization: Maximizing topological invariants, *Phys. Rev. B* **100**, 235452 (2019).
- [77] M. P. V. Stenberg, O. Köhn, and F. K. Wilhelm, Characterization of decohering quantum systems: Machine learning approach, *Phys. Rev. A* **93**, 012122 (2016).
- [78] J. Prasad and T. Souradeep, Cosmological parameter estimation using particle swarm optimization, *Phys. Rev. D* **85**, 123008 (2012).
- [79] Y.-H. Liu, Y. Zeng, Q.-S. Tan, D. Dong, F. Nori, and J.-Q. Liao, Optimal control of linear Gaussian quantum systems via quantum learning control, *Phys. Rev. A* **109**, 063508 (2024).
- [80] Y.-H. Liu and J.-Q. Liao, Mechanical quadrature squeezing beyond the 3 dB limit via quantum learning control, [arXiv:2404.13563](https://arxiv.org/abs/2404.13563).
- [81] H. Carmichael, *An Open Systems Approach to Quantum Optics* (Springer-Verlag, Berlin, Heidelberg, 1993).
- [82] J. R. Johansson, P. D. Nation, and F. Nori, QuTiP: An open-source Python framework for the dynamics of open quantum systems, *Comput. Phys. Commun.* **183**, 1760 (2012).
- [83] J. R. Johansson, P. D. Nation, and F. Nori, QuTiP 2: A Python framework for the dynamics of open quantum systems, *Comput. Phys. Commun.* **184**, 1234 (2013).
- [84] M. Aspelmeyer, T. J. Kippenberg, and F. Marquardt, Cavity optomechanics, *Rev. Mod. Phys.* **86**, 1391 (2014).